

Spin Fine Structure in Optically Excited Quantum Dot Molecules

M. Scheibner¹, M. F. Doty¹, I. V. Ponomarev¹, A.S. Bracker¹,
E.A. Stinnett¹, V.L. Korenev², T.L. Reinecke¹, and D. Gammon¹

¹Naval Research Laboratory, Washington, DC 20375, USA

²A.F. Ioffe Physical Technical Institute, St. Petersburg 194021 Russia

(Dated: December 2, 2024)

The interaction between spins in coupled quantum dots is revealed in distinct fine structure patterns in the measured optical spectra of InAs/GaAs double quantum dot molecules containing zero, one, or two excess holes. The fine structure is explained well in terms of a uniquely molecular interplay of spin exchange interactions, Pauli exclusion and orbital tunneling. This knowledge is critical for converting quantum dot molecule tunneling into a means of optically coupling not just orbitals but also spins.

PACS numbers: 78.67.Hc, 73.21.La, 78.47.+p, 78.55.Et

I. INTRODUCTION

Exchange coupling between spins in a double quantum dot molecule (QDM) is an essential component for spin-based quantum information^{1,2,3}. Rapid progress has been made recently in doubly charged QDMs that are measured and controlled electrically^{4,5}. A corresponding understanding of the spin-spin interactions in optically controlled QDMs is not yet available. These systems could lead to ultrafast, wireless control of spin qubits and optical entanglement of two spins in two dots. To this end it is now critical to obtain a detailed measurement and understanding of the spin states of optically excited QDMs.

In optically excited dots, an electron-hole (*e-h*) pair is created in the presence of the previously existing spin(s). As we will show, the resulting *e-e*, *h-h*, and *e-h* exchange interactions determine the spin states and can be directly measured through fine structure in the spectra^{6,7}. Moreover, *e* or *h* levels may be coupled by carrier tunneling in a QDM, with the orbital wavefunctions continuously tuneable from atomic to molecular in nature. Recently, photoluminescence (PL)

spectra of vertically-stacked InAs/GaAs QDMs measured as a function of electric field have led to the clear identification of tunnel coupling in neutral^{8,9,10,11,12,13} and charged QDMs.^{10,12,14,15}

Of great importance is the case of a doubly charged QDM because of its potential use as a two qubit system. To understand this system, we examine cases of zero, one and two charges in the QDM (see Fig. 1(a)). We demonstrate that all of the fine structure features of these systems arise from combinations of three fundamental quantum mechanical processes – tunneling, exchange, and Pauli exclusion. The neutral exciton, X^0 , illustrates *e-h* exchange in the presence of tunneling. The transition spectrum of the doubly positively charged exciton, X^{2+} , shows an effective *h-h* exchange splitting, which is created by tunneling and Pauli exclusion. For the singly charged exciton, X^+ , we find that the interplay of all these processes leads to an interesting ‘wiggling’ of a spectral line, which is a signature of the mixing of spin singlet and spin triplet states.

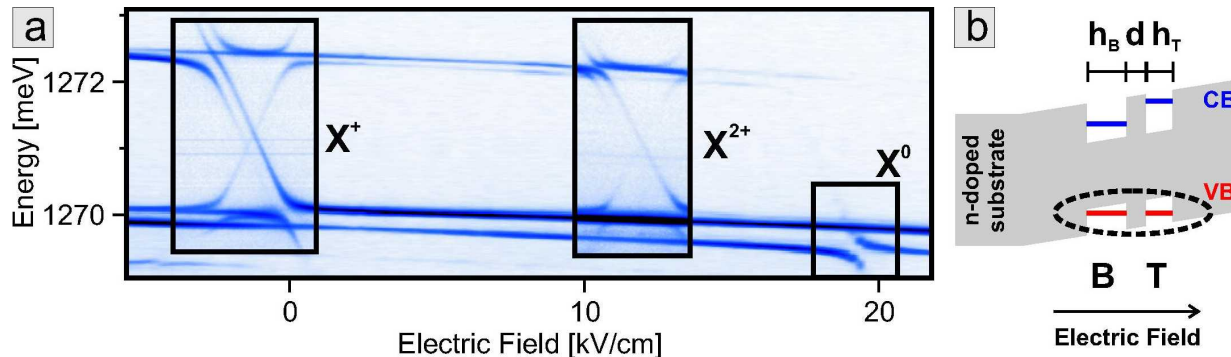


FIG. 1: (Color online) (a) Molecular resonances in the PL transitions of the neutral exciton (X^0), positive trion (X^+) and doubly positively charged exciton (X^{2+}) in a QDM. The bottom dot has a vertical height of $h_B = 4$ nm and the top dot has a vertical height of $h_T = 2.5$ nm with a dot separation of $d = 4$ nm. (b) Schematic of the QDM diode structure.

II. METHODS AND NOMENCLATURE

In the QDMs discussed here^{13,16} the hole levels are brought into resonance with an applied electric field, while the electron level of the top dot (T) is shifted to much higher energies relative to that of the bottom dot (B) (see Fig. 1(b)). Thus, we include in our discussion only the “atomic” s-shell orbital states for the electron localized in the bottom dot and for the holes in both dots. We consider samples with relatively wide interdot barriers ($d \geq 4$ nm) such that hole tunneling rates are small (≤ 1 meV). The QDMs were excited below the energy of the wetting layer. The interplay of optical excitation, recombination, and tunneling to the substrate leads to the observation of several charge states in the same spectrum. The PL was measured at 10 K with a resolution of 50 μ eV¹⁶.

To describe the quantum states of a QDM we use $_{eB(T)}^{eB(T)} X^q$, where $e_{B(T)}$ and $h_{B(T)}$ are the number of electrons and holes in the respective dot. For example, $_{21}^{10} X^{2+}$ for a doubly positively charged exciton, i.e., 1 e and 2 h 's in the bottom dot and 0 e and 1 h in the top dot. Likewise $_{21}^{10} X^{2+}$ corresponds to the indirect transition, $_{21}^{10} X^{2+} \Rightarrow _{20}^{00} h^{2+}$. We label specific spin states of a charge configuration as, e.g., $\uparrow\downarrow, \uparrow, \downarrow$, where we use the fact that a h in the ground state of a QD can take only two spin projections ($\uparrow, \downarrow \equiv \pm 3/2$), similar to the case of the spin-1/2 e (\uparrow, \downarrow)¹⁷. We specify the h spin singlet and triplet configurations as, e.g., $\uparrow\downarrow, \uparrow, \downarrow$ and $\uparrow\downarrow, \uparrow, \downarrow$ ¹⁸. The e 's and h 's are treated as non-identical particles with an explicit exchange interaction between them.

III. ELECTRON-HOLE EXCHANGE

A. The neutral exciton

We consider first the case of e - h exchange for the neutral exciton, $X^0 \equiv 1e + 1h$, in a QDM (Fig. 2). The exciton has spin states that are optically allowed (bright, $\uparrow\downarrow$ and $\downarrow\uparrow$), or optically forbidden (dark, $\uparrow\uparrow$ and $\downarrow\downarrow$)^{19,20}. In what follows we will not list spin degenerate states in which all spins, including the e spin, are flipped. At zero magnetic field a single intradot exciton line, $_{10}^{10} X^0$, anticrosses with the relatively weak interdot transition, $_{01}^{10} X^0$, with a splitting of $\Delta_{X^0} = 1.0$ meV (Fig. 2(a) top). When a transverse magnetic field of $B = 6$ T is applied (Voigt geometry) a second, normally dark, intradot spectral line appears 320 μ eV lower in energy (Fig. 2(a) bottom), because the transverse magnetic field mixes the bright and dark states²¹. The bright-dark splitting of the intradot exciton, $_{10}^{10} X^0$, arises from e - h exchange, similar to the case of a single dot. As the intradot exciton evolves into the interdot exciton through the anticrossing region, the e - h exchange splitting decreases substantially because of the decreased overlap of the e and h wavefunctions in the

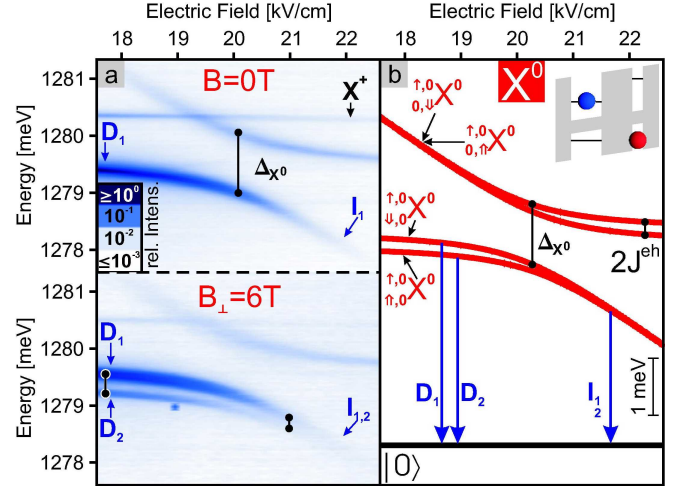


FIG. 2: (Color online) Exciton (X^0) in an uncharged QDM ($h_B = h_T = 2.5$ nm, $d = 4$ nm). (a) The PL spectrum as a function of electric field – at zero magnetic field ($B = 0$) (top) and in a transverse magnetic field ($B = 6$ T) (bottom) (b) The calculated energy diagram ($\Delta_{X^0} = 2t_h = 1.05$ meV, $2J^{eh} = 240$ μ eV). The direct exciton and its corresponding transition ($D_{1,2} \equiv _{10}^{10} X^0$) has the h in the same dot as the e and its energy is almost independent of electric field, while the indirect exciton ($I_{1,2} \equiv _{01}^{10} X^0$) has the h in the opposite dot and its energy changes linearly with field. An anticrossing occurs when their energies are resonant.

interdot configuration, $_{01}^{10} X^0$.

This physics is captured by calculations of the energy level structure as seen in Fig. 2(b), where we have included e - h exchange, J^{eh} , only for the intradot configurations $_{10}^{10} X^0$.²² Here the Hamiltonians of the bright ($_{10}^{10} X^0$, $_{0\downarrow}^{10} X^0$) and dark ($_{10}^{10} X^0$, $_{0\uparrow}^{10} X^0$) excitons at zero magnetic field are

$$\hat{H}_{b(d)}^{X^0} = \begin{pmatrix} \pm J^{eh} & t_h \\ t_h & -\gamma F \end{pmatrix}, \quad (1)$$

where energy and field are relative to the center of the exciton anticrossing and t_h is the single h tunneling rate²³. The applied electric field, F , changes the h energy in the top QD relative to that in the bottom QD by $\gamma F = e(d + (h_B + h_T)/2)F$ (e is the elementary charge, d is the separation of the dots and h_B , h_T are the heights of the dots). The neutral exciton exemplifies that in a QDM e - h exchange is large within the same dot but small between dots.

B. The doubly charged exciton

When we have two or more e 's (or h 's) we must also consider e - e (or h - h) interactions. The case of two e 's has been discussed for dots controlled by electrical gating.^{4,5,24} The case of two h 's is qualitatively the same and is observed optically in the doubly positively charged

exciton (X^{2+}). In contrast to the uncharged exciton, the doubly charged exciton transition shows an ‘x’-pattern¹⁰ with four anticrossings that involve two direct (A and D) and two indirect (B and C) transitions, as seen in Fig. 3(a). This transition pattern is understood using the calculated energy diagrams for the initial X^{2+} states and the final 2- h states left after recombination, which both have hole level resonances (Fig. 3(b)).

Each anticrossing has fine structure whose pattern provides a signature of the corresponding spin configurations. The two anticrossings on the left in the spectrum of Fig. 3(a) arise from the doubly charged exciton states ($\Delta_{X^{2+}}$) and those on the right from the 2- h states ($\Delta_{h^{2+}}$). We first consider the initial states of the X^{2+} transitions, as seen at the top of Fig. 3(b). With respect to spin, the X^{2+} states are qualitatively the same as the states of the neutral exciton. In particular, e - h exchange is present only when the electron shares the bottom dot with the unpaired hole, $^{10}_{12}X^{2+}$. The e - h exchange splitting decreases as the bottom QD is filled with two spin paired holes (total spin zero) and the top QD is left with an unpaired hole, $^{21}_{21}X^{2+}$. Note that this is visible in the X^{2+} transitions even without magnetic field (see Fig. 3(a) top left corner).

This is described by the Hamiltonian for the basis states $^{1,0}_{\downarrow\uparrow,\downarrow\downarrow}X^{2+}$, $^{1,0}_{\uparrow\uparrow,\downarrow\downarrow}X^{2+}$ (i) and $^{1,0}_{\uparrow\downarrow,\uparrow\uparrow}X^{2+}$, $^{1,0}_{\uparrow\downarrow,\uparrow\uparrow}X^{2+}$ (ii), which is similar to the Hamiltonian of the neutral exciton.

$$\hat{H}_{i(ii)}^{X^{2+}} = \begin{pmatrix} E_{BBT} & t_h \\ t_h & E_{BTT} \pm J^{eh} \end{pmatrix}, \quad (2)$$

where $E_{BBT} = -\gamma F$ and $E_{BTT} = V_{BB}^{eh} - V_{BT}^{eh} + V_{TT}^{hh} - V_{BB}^{hh} - 2\gamma F$. $V_{ik}^{\alpha\beta}$ denotes the direct Coulomb interaction between the two charges, α and β , when they are located in dot i and k respectively.²⁵

IV. ‘KINETIC’ EXCHANGE: TWO-HOLE STATES

If for the final state both h ’s are in the same dot ($^{00}_{02}h^{2+}$) the Pauli principle requires that there can be only a spin singlet state. On the other hand, if the h ’s are each in a different dot ($^{11}_{11}h^{2+}$) there will be a singlet and three triplet states. For large barrier width ($d \geq 4$ nm) the interdot h - h exchange is negligible, and the spin singlet and triplet states are degenerate at electric fields away from the anticrossing region. However, because tunneling conserves spin, only the interdot singlet configuration $^{0,0}_{\uparrow\downarrow}h_S^{2+}$ mixes with the intradot singlet $^{0,0}_{\downarrow\uparrow\downarrow}h_S^{2+}$, and the degenerate triplet states $^{00}_{11}h_T^{2+}$ pass through unaffected as shown in Fig 3(b). This is similar to the situation observed in transport experiments on the 2- e system^{4,5}. Mixing of the singlet states in the anticrossing region leads to an effective or ‘kinetic’²⁶ h - h exchange splitting between the singlet and the three degenerate triplets,

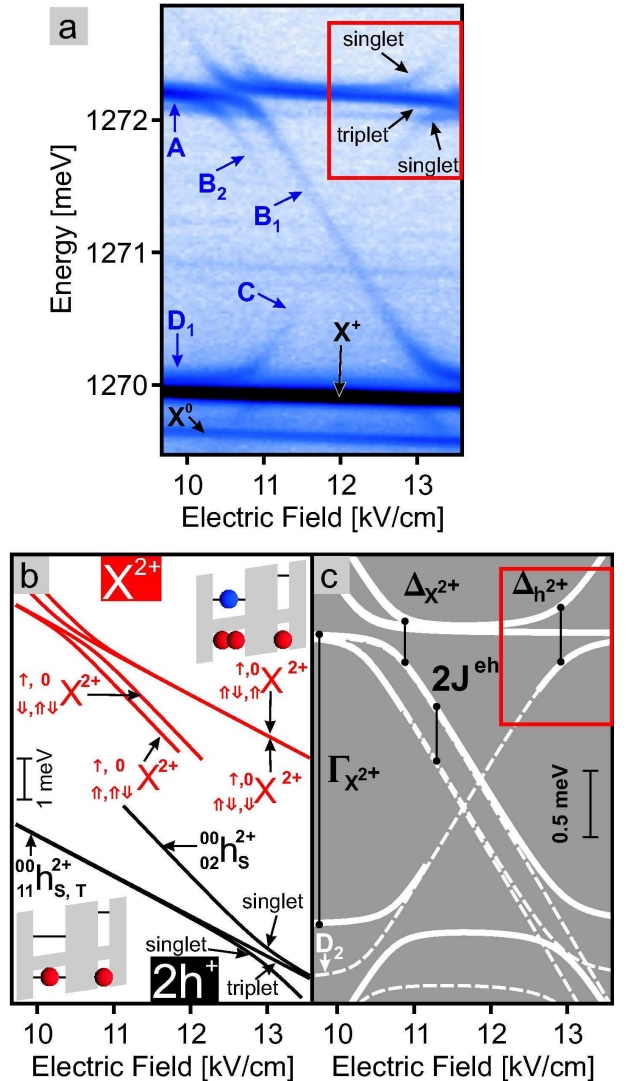


FIG. 3: (Color online) Doubly positively charged exciton (X^{2+}) in a QDM ($h_B = 4$ nm, $h_T = 2.5$ nm, $d = 4$ nm). (a) In the measured PL spectrum as a function of electric field an ‘x’-shaped pattern is formed by the X^{2+} transitions ($A \equiv {}^{10}_{21}X^{2+}$, $B \equiv {}^{10}_{12}X^{2+}$, $C \equiv {}^{10}_{21}X^{2+} \rightarrow {}^{00}_{02}h^{2+}$, $D \equiv {}^{10}_{11}X^{2+}$). (b) The calculated level diagram contains the states of the X^{2+} (red lines) and the 2- h states (h^{2+}) (black lines). The calculation is done using a fit to four parameters – t_h , J^{eh} , $\Gamma_{X^{2+}}$ ²⁵ and γ ($\Delta_{h^{2+}} = 2\sqrt{2}t_h = 410$ μ eV, $\Delta_{X^{2+}} = 2t_h = 310$ μ eV, $2J^{eh} = 410$ μ eV, $\Gamma_{X^{2+}} = 2.19$ meV, $\gamma = 0.99$ meV/(kV/cm)). Note that another 2- h state in which both h ’s are in the bottom dot exists, but is not seen in the displayed energy range. The two different field dependences seen in the 2- h and X^{2+} states lead to the field-independent direct (A and D) and field-dependent indirect (B and C) transitions. B and D are split by the e - h exchange J^{eh} of the optically excited state (X^{2+}). The red box in (a) marks an area where the singlet-triplet splitting of the two h resonance in (b) is reproduced nicely by the PL-signal. The anticrossing appears rotated because it occurs in the final state of the transitions (A and C). (c) Calculated PL spectrum. The solid lines resemble the spectrum in (a). The dashed lines map transitions that are optically weak or forbidden by optical selection rules.

even though interdot h - h exchange is negligible for wide barriers. This type of exchange, which is highly sensitive to the applied electric field through the resonant tunneling, provides a basis for externally manipulating the spin coupling.⁴

The Hamiltonian for the two relevant singlet states of the two h 's is

$$\hat{H}_S^{h^{2+}} = \begin{pmatrix} E_{TT} & \sqrt{2}t_h \\ \sqrt{2}t_h & E_{BT} \end{pmatrix}, \quad (3)$$

where $E_{TT} = V_{TT}^{hh} - 2\gamma F$ is the field dependent energy of the singlet ${}_{02}^{00}h_S^{2+}$ and $E_{BT} = V_{BT}^{hh} - \gamma F$ is the field dependent energy of the singlet, ${}_{11}^{00}h_S^{2+}$. The three decoupled triplet configurations, ${}_{11}^{00}h_T^{2+}$, also have the energy E_{BT} . The factor of $\sqrt{2}$ in the tunneling rate between the singlet states comes from the fact that two indistinguishable h 's can tunnel.¹⁰

Thus, the kinetic h - h exchange splitting arises in the 2- h energy diagram, and the e - h exchange splitting arises in the X^{2+} energy diagram. Therefore, the transition spectrum, which is the difference between the two energy diagrams, shows separately both types of spin fine structure (Fig. 3(a) and (c)).

Note, some transitions are optically weak (e.g. $B_2 \equiv {}_{\downarrow\downarrow\uparrow\uparrow}^{1,0}X^{2+}$) or forbidden by the optical selection rules (e.g. $D_2 \equiv {}_{\downarrow\downarrow\uparrow\uparrow}^{1,0}X^{2+}$) (white dashed lines in Fig. 3(c)), but become visible in the vicinity of anticrossings. There they gain some oscillator strength from states with optically stronger transitions.

V. INTERPLAY OF ELECTRON-HOLE AND KINETIC EXCHANGE: SINGLY CHARGED EXCITON

With the X^+ transitions we probe the QDM when it is charged with a single h (see Fig. 4). In the X^+ states kinetic h - h exchange and e - h exchange are both present and compete to determine the character of the spin state. In Fig. 4(a) the spectral pattern for the positive trion, X^+ , is shown. This pattern can be readily understood using the energy state diagrams in Fig. 4(b) of both the trion and the h that is left behind after recombination. We focus our discussion on the anticrossing pattern in the box in Fig. 4(a), in which an apparent triplet transition wiggles as it passes through the resonance.

At electric fields away from the anticrossing region, intradot e - h exchange determines the spin structure of the X^+ . That is, as shown in the top of Fig. 4(b), e - h exchange leads to a fine structure doublet with a splitting of $2J^{eh}$, much like the intradot X^0 case. The higher energy component consists of the e and one h in the bottom dot with their spins antiparallel (${}_{\downarrow\downarrow}^{1,0}X^+$, ${}_{\downarrow\downarrow}^{1,0}X^+$), while the lower energy component consists of parallel e and h spin in the bottom dot (${}_{\uparrow\downarrow}^{1,0}X^+$, ${}_{\uparrow\uparrow}^{1,0}X^+$).^{18,27}

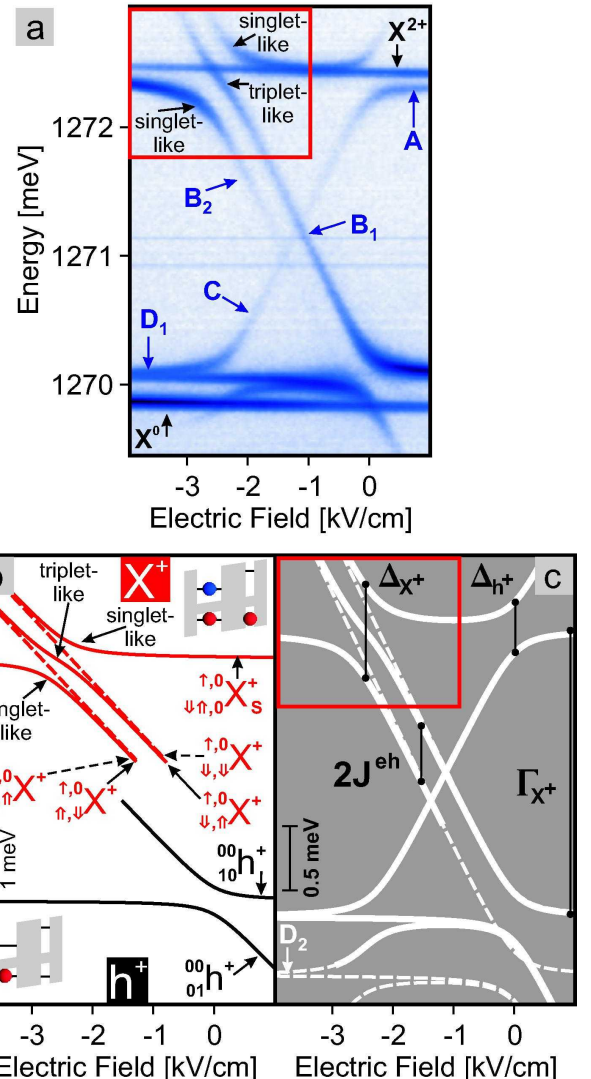


FIG. 4: (Color online) (a) In the measured PL spectrum as a function of electric field an 'x'-shaped pattern is formed by the X^+ transitions ($A \equiv {}_{20}^{10}X^+$, $B \equiv {}_{11}^{10}X^+$, $C \equiv {}_{11}^{10}X^+ \rightarrow {}_{01}^{00}h^+$, $D \equiv {}_{11}^{10}X^+$). (b) The calculated level diagram contains the states of the positive trion (X^+) (red lines) and the states of a single hole (h^+) (black lines) ($\Delta_{h^+} = 2t_{h^+} = 390 \mu\text{eV}$, $\Delta_{X^+} = 2\sqrt{2t_h^2 + (J^{eh})^2} = 750 \mu\text{eV}$, $2J^{eh} = 430 \mu\text{eV}$, $\Gamma_{X^+} = 2.21 \text{ meV}$, $\gamma = 0.99 \text{ meV}/(\text{kV}/\text{cm})$). Note that another X^+ state in which both h 's are in the top dot exists, but is not seen in the displayed energy range. The two different field dependences seen in the h^+ and X^+ states lead to the field-independent direct (A and D) and field-dependent indirect (B and C) transitions. B and D are split by the e - h exchange J^{eh} of the optically excited state (X^+). The red box in (a) marks an area where the singlet-triplet mixing at the X^+ resonance in (b) is reproduced nicely by the PL-signal. In the lower left corner of (a) the anticrossing is reproduced by the transitions D and C with different intensity ratios, but is partially covered by ${}_{10}^{10}X^0$. (c) Calculated PL spectrum. The solid lines resemble the spectrum in (a). The dashed lines map transitions that are optically weak or forbidden by optical selection rules.

As the electric field is tuned through the X^+ anticrossing region, tunnel coupling with the singlet $_{\uparrow\downarrow,0}^{1,0}X_S^+$ state forces the spin states ($_{\downarrow,\uparrow}^{1,0}X^+$, $_{\uparrow,\downarrow}^{1,0}X^+$) to form a h spin singlet-like state ($_{\downarrow,\uparrow}^{1,0}X_S^+$) and a h spin triplet-like state ($_{\downarrow,\uparrow}^{1,0}X_T^+$). This triplet would pass straight through the resonance (as with the 2- h states) except that e - h exchange continues to couple it to the singlets, causing it to shift continuously between the asymptotes determined by the e - h exchange splitting outside the anticrossing region. Essentially, in passing through the anticrossing region (from right to left) the $_{\downarrow,\uparrow}^{1,0}X^+$ state evolves continuously into the $_{\uparrow,\downarrow}^{1,0}X^+$ state through this triplet-like state.

The Hamiltonian that describes this behavior of the basis states $_{\uparrow\downarrow,0}^{1,0}X_S^+$, $_{\downarrow,\uparrow}^{1,0}X^+$ and $_{\uparrow,\downarrow}^{1,0}X^+$ is²⁷

$$\hat{H}_{\uparrow\downarrow}^{X^+} = \begin{pmatrix} E_{X^+} & t_h & t_h \\ t_h & E_{BT}^+ + J^{eh} & 0 \\ t_h & 0 & E_{BT}^+ - J^{eh} \end{pmatrix}. \quad (4)$$

With energy and field measured relative to the anticrossing of the h states, E_{X^+} is the energy of $_{\uparrow\downarrow,0}^{1,0}X_S^+$, $E_{BT}^+ \pm J^{eh} = E_{X^+} - \Gamma_{X^+} - \gamma F \pm J^{eh}$ are the energies of the states $_{\downarrow,\uparrow}^{1,0}X^+$ and $_{\uparrow,\downarrow}^{1,0}X^+$, and Γ_{X^+} determines the energy difference between the direct transitions A and D as shown in Fig. 4 (c). Again not all transitions between the X^+ states and the h^+ states are observed in the measured PL spectrum, because they are optically weak (e.g. $_{\downarrow,\downarrow}^{1,0}X^+$ (B_1)) or forbidden (e.g. $D_2 \equiv \underline{\underline{\downarrow,\uparrow}^{1,0}X^+}$) (Fig. 4(c), white dashed lines).

Tunneling and e - h exchange lead to a measured anticrossing energy $\Delta_{X^+} = 2\sqrt{2t_h^2 + (J^{eh})^2}$. The remaining h spin triplet states ($_{\downarrow,\downarrow}^{1,0}X^+$, $_{\uparrow,\uparrow}^{1,0}X^+$) retain their character and pass unaffected through the coupling region as shown in Fig. 4(b) (red dashed lines), because Pauli blocking prevents the h 's from tunneling. Thus, at the anticrossing point there is a kinetic exchange splitting between singlet- and triplet-like states, but e - h exchange splits the degeneracy between the triplet states and leads to a mixing between the singlets and one

of the triplets. Interestingly, the singlet-triplet mixing observed here is similar to that found in transport studies, but now mediated by e - h exchange instead of the hyperfine interaction^{4,5}.

VI. CONCLUSIONS

We have shown that the fine structure patterns measured in the optical spectra of QDMs are understood in detail in terms of the interplay between spin exchange and tunneling in the limit of wide barriers and negligible direct interdot exchange. Our description applies equally well to e tunneling and negatively charged QDMs. In addition we have measured the neutral biexciton, which is found to have spin structure qualitatively similar to the X^{2+} as expected. Interesting but more subtle effects such as fine structure due to asymmetries (e.g. lateral displacement of the dots) have for the most part remained below the resolution of our measurements. In cases where the barrier is relatively thin^{10,12,13} such that wave function overlap becomes large, we expect additional interactions (such as interdot exchange) to become significant.

An important implication of these results is that exchange is effectively turned off (or on) when the QDM is optically excited to specific spin states, thereby providing the opportunity for an ultrafast single qubit or 2-qubit operation. For example, the kinetic exchange interaction that splits the triplet and singlet states of the 2- h 's, $_{11}^{00}h^{2+}$, could be ‘optically gated’ for a well defined time by driving the QDM up and down through a $_{21}^{10}X^{2+}$ state (i.e. a virtual $_{21}^{10}X^{2+}$ transition).

Acknowledgments

We would like to acknowledge the financial support by NSA/ARO, CRDF, RFBR, RSSF, and ONR. M.F.D., I.V.P and E.A.S, are NRC/NRL Research Associates.

* Electronic address: scheibner@bloch.nrl.navy.mil

¹ D. Loss, D.P. DiVincenzo, Phys. Rev. A **57**, 120 (1998).

² D. P. DiVincenzo, D. Bacon, J. Kempe, G. Burkard and K. B. Whaley, Nature **408**, 339 (2000).

³ D. Awschalom, D. Loss and N. Samarth (eds.), *Semiconductor Spintronics and Quantum Computation* (Springer, 2002), ISBN 3540421769.

⁴ J. R. Petta, A. C. Johnson, J. M. Taylor, E. A. Laird, A. Yacoby, M. D. Lukin, C. M. Marcus, M. P. Hanson, and A. C. Gossard, Science **309**, 2180 (2005).

⁵ F. H. L. Koppens, J. A. Folk, J. M. Elzerman, R. Hanson, L. H. Willems van Beverem, I. T. Vink, H. P. Tranitz, W. Wegscheider, L. P. Kouwenhoven, and L. M. K. Vandersypen, Science **309**, 1346 (2005).

⁶ D. Gammon, E. S. Snow, B. V. Shanabrook, D. S. Katzer, and D. Park, Phys. Rev. Lett. **76**, 3005 (1996).

⁷ B. Urbaszek, R. J. Warburton, K. Karrai, B. D. Gerardot, P.M. Petroff, and J.M. Garcia, Phys. Rev. Lett. **90**, 247403 (2003).

⁸ H. J. Krenner, M. Sabathil, E. C. Clark, A. Kress, D. Schuh, M. Bichler, G. Abstreiter, and J. J. Finley, Phys. Rev. Lett. **94**, 057402 (2005).

⁹ G. Ortner, M. Bayer, Y. Lyanda-Geller, T. L. Reinecke, A. Kress, J. P. Reithmaier, and A. Forchel, Phys. Rev. Lett. **94**, 157401 (2005).

¹⁰ E. A. Stinaff, M. Scheibner, A. S. Bracker, I. V. Ponomarev, V. L. Korenev, M. E. Ware, M. F. Doty, T. L. Reinecke, D. Gammon, Science **311**, 636 (2006).

¹¹ T. Nakaoka, E. C. Clark, H. J. Krenner, M. Sabathil, M. Bichler, Y. Arakawa, G. Abstreiter, and J. J. Finley, Phys. Rev. B **74**, 121305 (2006).

¹² M. F. Doty, M. Scheibner, I.V. Ponomarev, E. A. Stinaff, A. S. Bracker, V. L. Korenev, T. L. Reinecke, and D. Gammon, Phys. Rev. Lett. **97**, 197202 (2006).

¹³ A. S. Bracker, M. Scheibner, M. F. Doty, E. A. Stinaff, I. V. Ponomarev, J. C. Kim, L. J. Whitman, T. L. Reinecke, and D. Gammon, Appl. Phys. Lett. **89**, 233110 (2006).

¹⁴ H. J. Krenner, E. C. Clark, T. Nakaoka, M. Bichler, C. Scheurer, G. Abstreiter, and J. J. Finley, Phys. Rev. Lett. **97**, 076403 (2006).

¹⁵ I. V. Ponomarev, M. Scheibner, E. A. Stinaff, A. S. Bracker, M. F. Doty, S. C. Badescu, M. E. Ware, V. L. Korenev, T. L. Reinecke, D. Gammon, phys. stat. sol. (b) **243**, 3869 (2006).

¹⁶ Further details on the growth and the experimental methods can be found in Ref.¹⁰.

¹⁷ K. V. Kavokin, Phys. Rev. B **69**, 075302 (2004).

¹⁸ $\uparrow, \downarrow \overset{\uparrow, 0}{X}_{S(T)}^+ \equiv \frac{1}{2} |B_1^h T_2^h \pm B_2^h T_1^h\rangle |\downarrow\downarrow\uparrow\downarrow \mp \downarrow\downarrow\uparrow\uparrow\rangle |B^e \uparrow\rangle$, where $B^{h(e)}$ and T^h denote the primary location of the orthonormal orbital wavefunctions of the e and the two h 's.

¹⁹ J. G. Tischler, A. S. Bracker, D. Gammon, and D. Park, Phys. Rev. B **66**, 081310(R) (2002).

²⁰ M. Bayer, G. Ortner, O. Stern, A. Kuther, A. A. Gorbutov, A. Forchel, P. Hawrylak, S. Fafard, K. Hinzer, T. L. Reinecke, S. N. Walck, J. P. Reithmaier, F. Klopff, and F. Schäfer, Phys. Rev. B **65**, 195315 (2002).

²¹ M. Bayer, O. Stern, A. Kuther, A. Forchel, Phys. Rev. B **61**, 7273 (2000).

²² $e - h$ exchange can be modeled as a short range interaction: $\hat{J}_{ij}^{eh} = A \sum_{i,j} \delta(\mathbf{r}_{ei} - \mathbf{r}_{hj}) \hat{\sigma}_{iz}^e \hat{\sigma}_{jz}^h$, where i and $j = B, T$ and A is a coupling constant. The matrix element is $J^{eh} \equiv J_{BB}^{eh} = A \int d\mathbf{r} |\varphi_B^e| |\varphi_B^h|^2$, where $\varphi_B^{e(h)}$ are the orthonormalized wavefunctions of e and h in the bottom dot only.

²³ For wide barriers contributions to the tunneling rate due to the presence of additional charges are negligible¹⁰.

²⁴ G. Burkard, G. Seelig and D. Loss, Phys. Rev. B **62**, 2581 (2000).

²⁵ $\Gamma_{X^{2+}} = \Gamma_{X^+} = V_{BT}^{eh} - V_{BB}^{eh} + V_{BB}^{hh} - V_{BT}^{hh} - J^{eh}$. $V_{ij}^{\alpha\beta} \equiv V_{iijj}^{\alpha\beta}$ denote the direct Coulomb potentials between the charges α and β primarily located in dot i and j respectively, where: $V_{ijkl}^{\alpha,\beta} = \pm \int d\mathbf{r} d\mathbf{r}' |\mathbf{r} - \mathbf{r}'|^{-1} \varphi_i^{\alpha*}(\mathbf{r}) \varphi_j^{\beta*}(\mathbf{r}') \varphi_j^{\alpha}(\mathbf{r}) \varphi_l^{\beta}(\mathbf{r}')$, with the orthonormalized wavefunction φ_i^{α} of particle α in dot i .

²⁶ P. Fazekas, *Lecture Notes on Electron Correlation and Magnetism* (World Scientific, Singapore, 1999).

²⁷ We define: $\overset{\uparrow, 0}{X}_{\uparrow\downarrow}^+ = \frac{1}{\sqrt{2}} (\overset{\uparrow, 0}{X}_S^+ + \overset{\uparrow, 0}{X}_T^+)$ and $\overset{\uparrow, 0}{X}_{\uparrow\downarrow}^+ = \frac{1}{\sqrt{2}} (\overset{\uparrow, 0}{X}_S^+ - \overset{\uparrow, 0}{X}_T^+)$. In Ref.¹⁰ $\overset{\uparrow, 0}{X}_{\uparrow\downarrow, 0}^+$, $\overset{\uparrow, 0}{X}_S^+$ and $\overset{\uparrow, 0}{X}_T^+$ were used as basis states. In this basis Eqn. (4) would be

$$\hat{H}_{\uparrow\downarrow}^{X^+} = \begin{pmatrix} E_{X^+} & \sqrt{2}t_h & 0 \\ \sqrt{2}t_h & E_{BT}^+ & J^{eh} \\ 0 & J^{eh} & E_{BT}^+ \end{pmatrix}.$$

.